



HAL
open science

Mapping thermal emission in the synchrotron-dominated SNRs 330.2+1.0, 3C58, and RX J1713.7-3946

Adrien Picquenot, Brian J Williams, Fabio Acero, Koji Mori

► **To cite this version:**

Adrien Picquenot, Brian J Williams, Fabio Acero, Koji Mori. Mapping thermal emission in the synchrotron-dominated SNRs 330.2+1.0, 3C58, and RX J1713.7-3946. *Astron.Astrophys.*, 2024, 683, pp.A197. 10.1051/0004-6361/202348246 . hal-04455652

HAL Id: hal-04455652

<https://hal.science/hal-04455652v1>

Submitted on 20 Apr 2024




HAL is a multi-disciplinary open access archive for the deposit and dissemination of scientific research documents, whether they are published or not. The documents may come from teaching and research institutions in France or abroad, or from public or private research centers.

L'archive ouverte pluridisciplinaire **HAL**, est destinée au dépôt et à la diffusion de documents scientifiques de niveau recherche, publiés ou non, émanant des établissements d'enseignement et de recherche français ou étrangers, des laboratoires publics ou privés.



Distributed under a Creative Commons Attribution 4.0 International License

Mapping thermal emission in the synchrotron-dominated supernova remnants G330.2+1.0, 3C58, and RX J1713.7-3946

A. Picquenot^{1,2,3} , B. J. Williams² , F. Acero^{4,5} , and K. Mori^{6,7}

¹ Department of Astronomy, University of Maryland, College Park, MD 20742, USA
e-mail: app46.pr@gmail.com

² X-ray Astrophysics Laboratory NASA/GSFC, Greenbelt, MD 20771, USA

³ Center for Research and Exploration in Space Science and Technology, NASA/GSFC, Greenbelt, MD 20771, USA

⁴ Université Paris-Saclay, Université Paris-Cité, CEA, CNRS, AIM, 91191 Gif-sur-Yvette, France

⁵ FSLAC IRL 2009, CNRS/IAC, La Laguna, Tenerife, Spain

⁶ Department of Applied Physics and Electronic Engineering, University of Miyazaki, 1-1, Gakuen Kibanadai-nishi, Miyazaki 889-2192, Japan

⁷ Institute of Space and Astronautical Science (ISAS), Japan Aerospace Exploration Agency (JAXA), Japan

Received 12 October 2023 / Accepted 22 January 2024

ABSTRACT

Aims. Since the discovery of synchrotron X-ray emission from the shell of the supernova remnant (SNR) SN 1006, multiple observations from *Chandra* and *XMM-Newton* have shown that many young SNRs produce synchrotron emission in X-rays. Among those, a few peculiar SNRs have their X-ray emission largely dominated by synchrotron radiation, showing no or only faint traces of thermal emission. In this paper, we report our mapping of the thermal emission in three emblematic synchrotron-dominated SNRs: G330.2+1.0, 3C58, and RX J1713.7-3946.

Methods. We used a blind source separation method able to retrieve faint components from X-ray data in the form of *Chandra* and *XMM-Newton* observations. The thermal candidates disentangled by the algorithm were then used to select regions of extraction. We then analyzed the extracted spectra to assess their physical nature.

Results. We conclude that the components retrieved by the algorithm indeed represent the spatial distribution of the thermal emission in G330.2+1.0 and 3C58, and a likely thermal candidate in RX J1713.7-3946. Our findings confirm and expand on past studies.

Key words. ISM: lines and bands – ISM: structure – ISM: supernova remnants – X-rays: individuals: G330.2+1.0 – X-rays: individuals: 3C58 – X-rays: individuals: RX J1713.7-3946

1. Introduction

Since the discovery of synchrotron X-ray emission from the shell of SN 1006 (Koyama et al. 1995), multiple observations from *Chandra* and *XMM-Newton* have shown that many young supernova remnants (SNRs) produce synchrotron emission in X-rays. Among those, a few peculiar SNRs have their X-ray emission largely dominated by synchrotron radiation, showing no or only faint traces of thermal emission.

Of these synchrotron-dominated SNRs, the remnant of SN 1054, dominated by the pulsar wind nebula (PWN) known as the Crab, is the most notorious example: despite numerous attempts (e.g., Seward et al. 2006; Hitomi Collaboration 2018), no evidence of thermal emission has ever been found. G330.2+1.0, the SNR surrounding 3C58, and RX J1713.7-3946 are emblematic synchrotron-dominated SNRs in which traces of thermal emission have been detected in previous studies.

G330.2+1.0 is a synchrotron-dominated SNR showing a clear shell in X-rays, and harbors a central compact object (CCO; Park et al. 2006), presumably a neutron star. Its age has been estimated to be less than about 1000 yr by Borkowski et al. (2018).

The PWN 3C58 harbors a 66 ms pulsar in its center, and presents axisymmetric lobes. It has been linked to the SN explosion observed in A.D. 1181 by Chinese and Japanese astronomers (Stephenson 1971), but it has also been argued that some of its

characteristics were indicative of a much older age (see e.g., Roberts et al. 1993). However, a new distance estimate of 2 kpc instead of the traditionally accepted 3.2 kpc would be consistent with an age of ~840 yr (Kothés 2013).

RX J1713.7-3946 is a shell-type SNR, and the brightest X-ray synchrotron and TeV gamma-ray SNR in our Galaxy. Wang et al. (1997) proposed that RX J1713.7-3946 could be the remnant of the SN that exploded in A.D. 393.

In Park et al. (2009) and Williams et al. (2018), a small region to the east of G330.2+1.0 was found to be a source of thermal emission. Bocchino et al. (2001), Slane et al. (2004), and Gotthelf et al. (2007) detected evidence of thermal emission in 3C58, the latter producing a synchrotron-subtracted image of the remnant using stacked *XMM-Newton* observations. Finally, thermal emission was detected in a central region of RX J1713.7-3946 by Katsuda et al. (2015) after numerous unsuccessful or debated attempts (e.g., Koyama et al. 1997; Slane et al. 1999; Pannuti et al. 2003). However, these past studies mainly focused on the spectral analysis of small regions within the remnants and, with the exception of the synchrotron-subtracted map of Gotthelf et al. (2007), there was no real attempt to probe the global spatial distribution of thermal emission in these SNRs.

In this paper, we propose a different approach to tackling the problem: we attempt to map the thermal emission in G330.2+1.0, 3C58, and RX J1713.7-3946 with a new method. In Sect. 2, we present our image-extraction method, while the following

Table 1. Data from *XMM-Newton* and *Chandra* used in our study.

Object	ObsID	Date	Exposure (ks)			
			MOS 1	MOS 2	pn	ACIS-S
G330	0742050101	2015 Mar. 8	112.4	109.3	111.2	–
3C58	728	2000 Sep. 4	–	–	–	50.0
	3832	2003 Apr. 26	–	–	–	135.8
	4382	2003 Apr. 23	–	–	–	167.4
	4383	2003 Apr. 22	–	–	–	38.7
		Total	–	–	–	391.9
RX J1713	0093670501	2001 Mar. 02	11.6	11.6	6.5	–
	0203470501	2004 Mar. 25	13.6	13.6	9.4	–
	0740830201	2014 Mar. 2	89.5	89.5	–	–
	0743030101	2015 Mar. 10	67.0	67.0	38.3	–
	0804300901	2017 Aug. 29	19.5	19.5	14.2	–
	0804300801	2017 Aug. 30	43.6	43.6	33.0	–
	0804301001	2018 Mar. 23	50.6	52.3	32.2	–
	0804300301	2018 Mar. 29	55.7	55.7	34.1	–
	0804300401	2018 Mar. 31	51.5	51.5	28.0	–
	0804300501	2018 Mar. 25	97.5	97.6	55.1	–
	0804300601	2018 Mar. 19	49.8	49.8	38.7	–
	0804300701	2018 Mar. 21	70.7	70.7	41.4	–
	0804300101	2018 Aug. 26	69.7	69.7	53.7	–
		Total	690.3	692.1	384.6	–

Notes. EPIC exposure times are after filtering.

sections present our results for G330.2+1.0, 3C58, and RX J1713.7-3946, respectively.

2. Method

To retrieve accurate maps of the thermal emission in the three synchrotron-dominated SNRs we propose to study, we used a blind source separation (BSS) method based on the general morphological components analysis (GMCA; see [Bobin et al. 2015](#)) first introduced for X-ray observations by [Picquenot et al. \(2019\)](#). This algorithm can disentangle spectrally and spatially mixed components from an X-ray data cube of the form (x, y, E) . In particular, the algorithm was shown to be able to extract extremely faint components from X-ray data cubes. The outputs take the form of an image associated with a mean spectrum for each component. As the algorithm primarily focuses on spatial morphological features without the help of any prior physical information, the extracted spectra can sometimes appear poorly reconstructed, particularly for faint components. These spectra can nonetheless provide hints regarding the nature of the extracted component, and the images can be used to extract a spectrum from the original data in the region of interest. The GMCA algorithm can therefore be used as an effective complementary tool for the search for faint emission within spatially resolute sources. An updated version, the pGMCA (see [Bobin et al. 2020](#)), has been developed to take into account the Poissonian nature of X-ray data. It was first used on Cas A SNR data from *Chandra* and proved to be perfectly suited for producing clear, detailed, and unpolluted images of both the ejecta ([Picquenot et al. 2021](#)) and the synchrotron at different energies ([Picquenot et al. 2023](#)).

In the present study, we used pGMCA on stacked *Chandra* observations of 3C58 and, for the first time, on an *XMM-Newton*

observation of G330.2+1.0. As the algorithm does not handle mosaic data with highly uneven exposure maps, we combined *XMM-Newton* observations of the large RX J1713.7-3946 remnants, corrected the exposure, and removed the background and solar flares to generate a flux data cube. We also removed the CCOs from all the remnants with an inpainting method using wavelet transforms in order to alleviate the signal intensity contrast.

3. G330.2+1.0

To study G330.2+1.0, we used the *XMM-Newton* 0742050101 observation (see Table 1). We reprocessed the data and removed the solar flares using the dedicated *SAS* routines, and stacked MOS1, MOS2, and pn observations in a (x, y, E) data cube. We chose a 6'' spatial binning and a 116.8 eV energy binning to increase the photon counts in each bin. We removed the CCO using an inpainting method.

The pGMCA algorithm was able to retrieve two meaningful components shown in Fig. 1. We identify these as synchrotron and thermal emission, respectively. The component we identified as thermal was associated with a spectrum endowed with thermal features but too poorly reconstructed to be used as such in a detailed spectral analysis (see the bottom right panel of Fig. 2 for an example of spectra retrieved by pGMCA). Figure 1 also shows a three-color image of G330.2+1.0 on which the contours of our thermal emission are overlaid. It appears that these contours highlight the region shown in Fig. 4 (east region) of [Park et al. \(2009\)](#) and Fig. 1 of [Williams et al. \(2018\)](#), where both studies detected thermal emission. We did not carry out any spectral analysis of this region as this has already been done extensively by [Williams et al. \(2018\)](#).

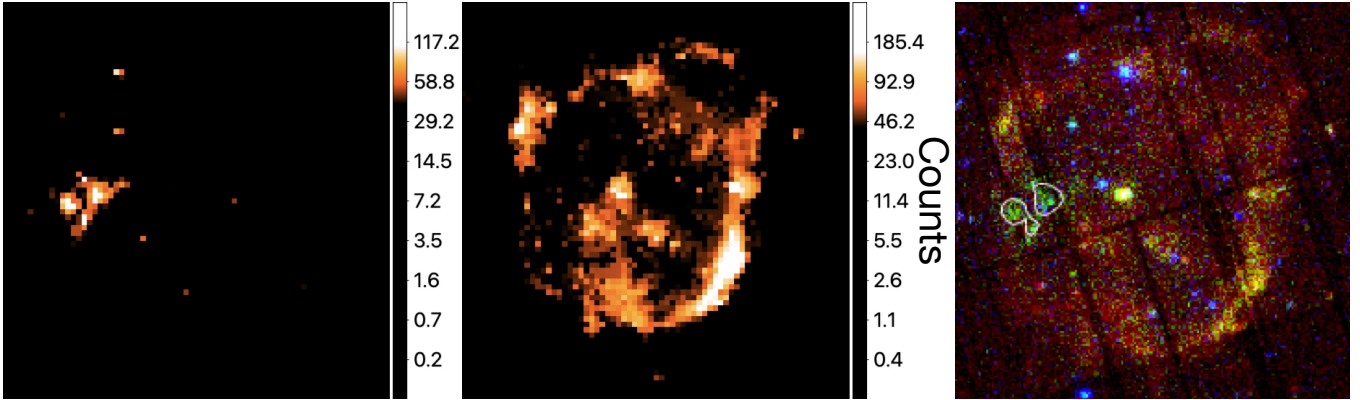


Fig. 1. Thermal emission distribution in G330.2+1.0. The component retrieved by pGMCA that we identify as thermal emission is shown on the left. In the middle, we show the component retrieved by pGMCA that we identify as synchrotron emission. On the right, we show an *XMM-Newton* three-color image of G330.2+1.0, with 0.4–1.2 keV emission in red, 1.2–2.0 keV emission in green, and 2.0–7.0 keV emission in blue. The contours of our thermal emission component are overlaid in white; they appear in the green clump region that was studied in Williams et al. (2018) and shown to harbor thermal emission. The scales are logarithmic.

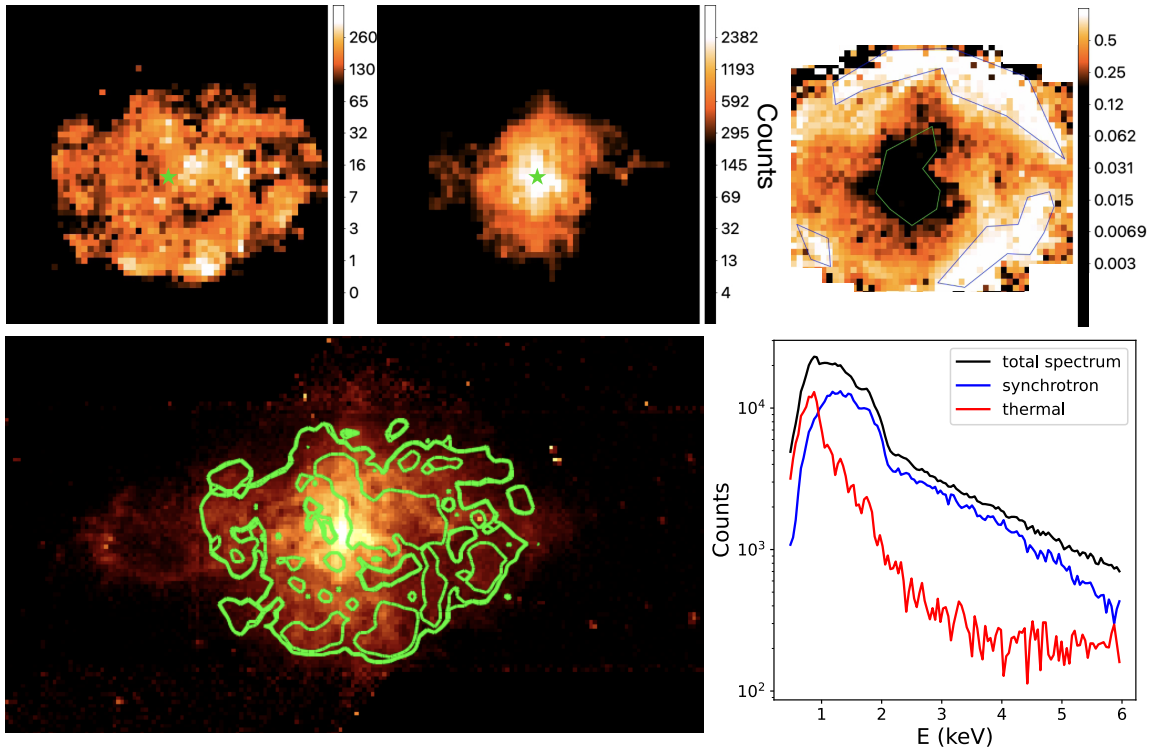


Fig. 2. Thermal emission distribution in 3C58. In the top left panel, we show the component retrieved by pGMCA that we identify as thermal emission. In the middle, we show the main component retrieved by pGMCA that we identify as synchrotron emission. The green stars highlight the pulsar position. On the right, we present a ratio map thermal/(thermal+synchrotron). The regions we used to extract a spectrum are overlaid in blue (thermal) and green (synchrotron). In the bottom left, we show a broadband flux image of 3C58 obtained using the merge_obs routine from CIAO, which is superimposed with the contours from the thermal emission. For all the images, the scales are logarithmic. In the bottom right panel, we show spectra retrieved by pGMCA associated to the thermal and synchrotron emissions.

The pGMCA algorithm did not find any other meaningful component that could be interpreted as thermal emission, and we observed that the spatial distribution of the thermal and synchrotron emissions are clearly anti-correlated. Furthermore, the synchrotron component appears slightly recessed around the thermal region, which supports the interpretation of Williams et al. (2018) that most of the blast wave is encountering very

low-density material, while a small section encounters a denser region of either the interstellar medium (ISM) or a clump of circumstellar material (CSM). The results obtained using pGMCA on this remnant can be seen as a methodological test as they confirmed past studies, without significantly expanding on them. The major novelty here would be a nondetection: there does not seem to be any other thermal emission than that in the

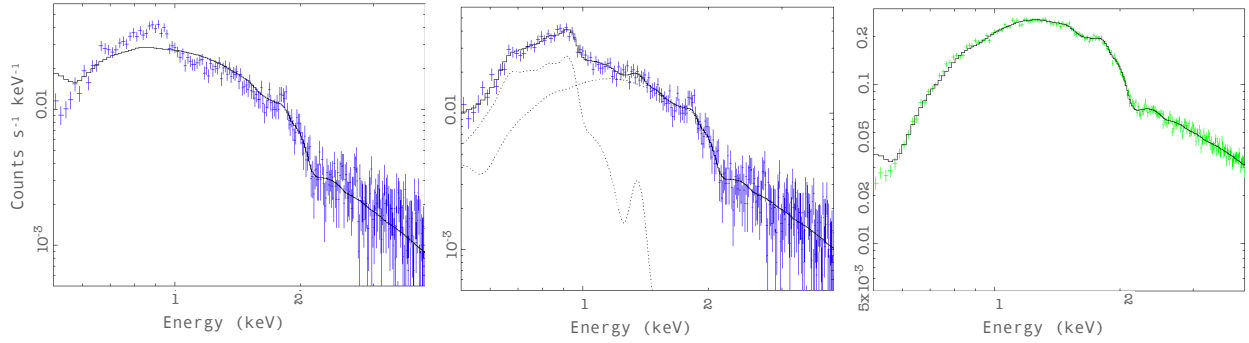


Fig. 3. Background-subtracted spectra extracted from the thermal and synchrotron-dominated regions from the right panel of Fig. 2. On the left, we show the spectrum extracted from the thermal region fitted with a `phabs(powerlaw)` model in Xspec. In the middle, we show the same thermal spectrum fitted with a `phabs(powerlaw+vnei)` model. Best-fit parameters of this model are shown in Table 2. On the right, we show the spectrum extracted from the synchrotron-dominated region fitted with a simple `phabs(powerlaw)` model.

eastern region, which would favor the interpretation that we are observing a clump of ISM or CSM.

4. 3C58

To study 3C58, we used *Chandra* 728, 3832, 4382, and 4383 ACIS observations (see Table 1). We reprocessed the data with CIAO v4.15, and stacked the observations in a (x, y, E) data cube. We chose a $30''$ spatial binning and a 43.8 eV energy binning to increase the photon counts in each bin. We removed the pulsar using an inpainting method. We used *Chandra* observations rather than *XMM* because the better resolution allowed a spatial rebinning to increase the statistics, without losing too much morphological information.

The pGMCA algorithm was able to retrieve two meaningful components shown in Fig. 2 that we identify respectively as synchrotron and thermal emission. The component we identified as thermal was associated with a spectrum endowed with thermal features, as can be seen in the bottom right panel of Fig. 2. The global shape is consistent with a thermal spectrum, but it is too poorly reconstructed to be used as such in a detailed spectral analysis. To assess the thermal nature of the latter, we therefore defined extraction regions by eye based on the ratio map presented in the top right panel of Fig. 2. The resulting background-subtracted spectra are presented in Fig. 3.

We used the spectral fitting package Xspec to fit the spectrum of the thermal candidate with a `phabs(powerlaw+vnei)` model, and compared the results with a simple `phabs(powerlaw)` model, as shown in Fig. 3. This spectrum clearly contains thermal emission, and the results of our best fit for the `phabs(powerlaw+vnei)` model are shown in Table 2. Similarly, fitting a `phabs(powerlaw)` model on the synchrotron spectrum confirms the spatial distribution of the thermal and synchrotron components disentangled by pGMCA.

Our results are consistent with the studies from Gotthelf et al. (2007) and Slane et al. (2004), where an overabundance of Ne IX was detected. Our thermal map also appears similar to the synchrotron-subtracted image shown in Fig. 8 of Gotthelf et al. (2007). Using a BSS method allowed the disentanglement of a crisper, cleaner image of this faint thermal component surrounding the core of the synchrotron emission.

The nature of this thermal component has been discussed in previous studies. Slane et al. (2004) hypothesized that the overabundance of Ne indicates that this component is composed of ejecta, but Gotthelf et al. (2007) argue that the solar

Table 2. Best fits obtained in Xspec to describe the thermal-dominated spectrum from the central panel of Fig. 3, with a `phabs(powerlaw+vnei)` model.

Model	Parameter	Best fit
<code>phabs</code>	N_{H} (10^{22} cm $^{-2}$)	0.42 ± 0.07
<code>powerlaw</code>	PhoIndex	2.55 ± 0.05
	norm	$8.95\text{E-}05 \pm 3.3\text{E-}06$
<code>vnei</code>	kT (keV)	0.25 ± 0.06
	τ (s cm $^{-3}$)	$2.4\text{E+}11 \pm 4.5\text{E+}11$
	norm	$1.41\text{E-}04 \pm 1.5\text{E-}04$
	O	0.583 ± 0.29
	Ne	1.84 ± 0.66
	Mg	1.43 ± 0.63

abundance of Ne has been systematically underestimated by a factor of two (Cunha et al. 2006). Bietenholz et al. (2013) propose two arguments against the thermal emission being ejecta based on results from Gotthelf et al. (2007) that are consistent with the findings of the present study. The geometrical center of the thermal component from Gotthelf et al. (2007) is offset from the current pulsar position and its projected origin, and the thermal emission (~ 5.6 pc E–W extent) appears to be smaller than the PWN (~ 8.5 pc E–W extent). While we think that the circular approximation made by Gotthelf et al. (2007) to describe the shape of the thermal emission is too coarse and that the argument in favor of a geometrical center is unconvincing as it relies on a spherical evolution assumption, we find the component we extracted to be of a similar 5.6 pc E–W extent.

The bottom panel of Fig. 2 shows the contours of the thermal emission superimposed on a synchrotron-dominated broadband flux image of the PWN obtained using the `merge_obs` routine from CIAO. There is no clear correlation between the thermal component and the filaments from the synchrotron emission, which suggests that there is no interaction between the thermal and nonthermal plasma. The thermal component is therefore likely of ISM origin; it could be ejecta, but only if the reverse shock has not yet reached the center of the remnant.

5. RX J1713.7-3946

RX J1713.7-3946 is a large SNR with $\sim 1^\circ$ diameter, meaning a collection of *XMM-Newton* observations (see Table 1) is required

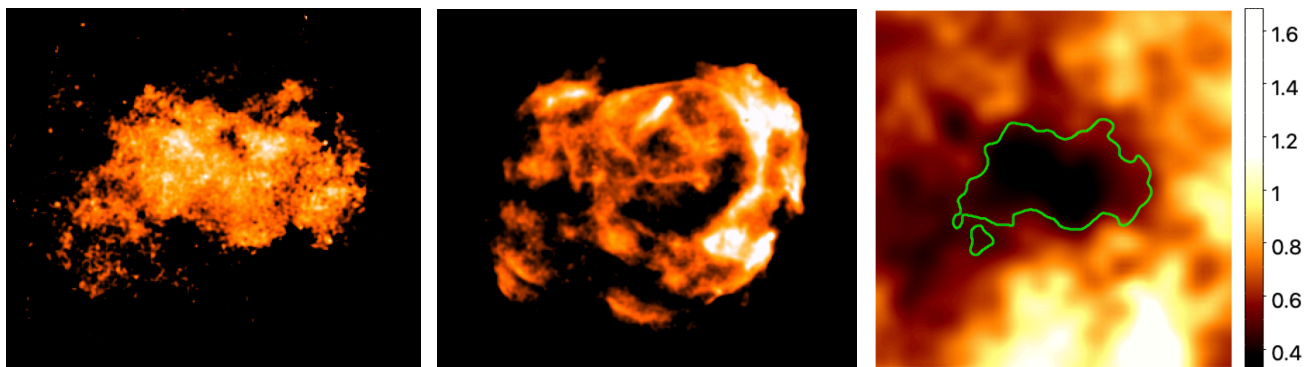


Fig. 4. Thermal candidate distribution in RX J1713.7-3946. On the left, we show the component retrieved by GMCA that we identify as potential thermal emission. In the middle, we show the component retrieved by GMCA that we identify as synchrotron emission. The scales are logarithmic. The compact object in the center has been masked. On the right, we show the column density map derived from optical extinction (in units of 10^{22} cm^{-2}), over which we superimpose the contour of our thermal candidate.

to map the entire remnant. The data were processed differently from the two previous targets presented in this study. These deep observations were combined to produce a mosaic data cube with fine energy binning. The energy range 0.5–10 keV was divided into 18 energy bands in logarithmic space resulting in energy bins of ~ 100 eV below 1 keV and ~ 500 eV at 3 keV. The spatial bin size is of $16''$. Each energy band gave a distinct image that was processed individually in a similar way to that described in [Acero et al. \(2009\)](#), except for the fact that filter wheel closed background files¹ were used instead of blank sky event files. For each observation, for each instrument, and for each energy band, the counts map is subtracted from the filter wheel closed background; the resulting images for all instruments and all observations are then assembled in a mosaic and finally divided by the corresponding mosaic exposure map. The final cube is reassembled using the processed images as “energy slices”. Contrary to the data cubes used to study 3C58 and G330.2+1.0, the cube resulting from this process is in flux units instead of counts. For that reason, we used the GMCA algorithm instead of pGMCA, as this latter is only suited for Poissonian data sets.

Faint thermal emission was previously reported by [Katsuda et al. \(2015\)](#) in the center of the SNR where deep exposures dedicated to the compact object were available. If this thermal emission were part of a larger structure, we might expect the GMCA to disentangle the synchrotron-dominated part from the thermal component in a full coverage data set. The GMCA algorithm was indeed able to retrieve two components at lower energies shown in Fig. 4, which we identify respectively as synchrotron and potential thermal emission. The spectrum of the potential thermal emission only consists of a small peak at lower energies. In this case, the identification of the fainter component with thermal emission is not obvious, as a spectral analysis similar to the one we conducted for 3C58 did not lead to robust results. In the spectrum extracted from the central region, which is the brightest in our thermal candidate/synchrotron ratio map, we found faint traces of thermal emission at low energies, as reported by [Katsuda et al. \(2015\)](#).

We note that [Pannuti et al. \(2003\)](#) also claimed to have detected traces of thermal emission in the diffuse emission from the remnant but not in the bright northwestern rim. Our thermal candidate does not show any emission in this region either

(see Fig. 1 of [Pannuti et al. 2003](#)). Similar findings of softer emission in the center than to the northwest were reported by [Cassam-Chenaï et al. \(2004\)](#). However, spectra extracted from regions where our thermal candidate is supposed to be present but where the ratio is lower than in the center do not show significant traces of thermal emission. The identification of our thermal candidate is therefore uncertain.

The fact that the brightest part in our thermal candidate appears at low energies in the only region where thermal emission has been observed with certainty favors its identification as a thermal component. However, our thermal candidate could also be synchrotron emission endowed with an absorption column density and/or spectral index sufficiently different from the main synchrotron component to be separated from it by the algorithm as a spectrally and morphologically distinct source. To test the hypothesis of a spatially different absorption effect, we built a map of the X-ray absorption N_{H} using the optical extinction map A_{V} from [Dobashi et al. \(2005\)](#). We used a conversion factor between hydrogen column density and optical extinction $N_{\text{H}} (\text{cm}^{-2}) = 2.21 \times 10^{21} A_{\text{V}}$ ([Güver & Özel 2009](#)). We are aware that the absorption map derived from extinction has several limitations; one being that the N_{H} map is not restricted to the SNR distance. Nonetheless, [Sano et al. \(2015\)](#) showed that there is a good correlation between the measured X-ray N_{H} and the optical extinction (see Fig. 4).

The resulting absorption map is shown in the right panel of Fig. 4, and shows lower absorption in the center region and higher absorption towards the outer parts of the SNR. This map bears morphological similarities to our thermal candidate map. Therefore, this component could either be of thermal origin, more visible in the center as it is less absorbed at lower energies, or synchrotron emission endowed with a different spectral index and a lower absorption. Both effects could also play a role, and the GMCA might separate a mixed component, containing traces of thermal and nonthermal emission. Further studies would be necessary to assess the origin of this component with more confidence.

6. Conclusions

The use of the GMCA and pGMCA algorithms allowed a detailed mapping of thermal emission in the synchrotron-dominated remnants G330.2+1.0 and 3C58, and led to the discovery of a thermal candidate in RX J1713.7-3946.

¹ <https://www.cosmos.esa.int/web/xmm-newton/filter-closed>

In G330.2+1.0, the thermal emission appears localized in the same region studied in Williams et al. (2018), supporting the idea that most of the blast wave is encountering very low-density material, while a small section encounters a denser region of either the ISM or a clump of CSM.

In 3C58, the thermal emission surrounds the X-ray-bright central region, but appears significantly smaller than the PWN (~5.6 pc against ~8.5 pc E–W extent). The nature of this emission has been discussed in previous studies, and these latter mostly consider it to be ISM rather than heated ejecta. Our results are consistent with this conclusion.

In RX J1713.7-3946, the GMCA algorithm retrieved a component in lower energies that could be thermal emission, but we cannot identify this with certainty. The brightest region was shown by Katsuda et al. (2015) to harbor spatial emission at lower energies, and its spatial distribution is highly different from that of the synchrotron, favoring a thermal origin. We find no clear signs of thermal emission in the spectra extracted from other regions.

Acknowledgements. The material is based upon work supported by NASA under award number 80GSFC21M0002. The research leading to these results has received funding from the European Union’s Horizon 2020 Program under the AHEAD2020 project (grant agreement no. 871158). This work was supported by CNES, focused on methodology for X-ray analysis.

References

- Acero, F., Ballet, J., Decourchelle, A., et al. 2009, *A&A*, 505, 157
 Bietenholz, M. F., Kondratiev, V., Ransom, S., et al. 2013, *MNRAS*, 431, 2590
 Bobin, J., Rapin, J., Larue, A., & Starck, J.-L. 2015, *IEEE Trans. Signal Process.*, 63, 1199
 Bobin, J., Hamzaoui, I. E., Picquenot, A., & Acero, F. 2020, *IEEE Trans. Image Process.*, 29, 9429
 Bocchino, F., Warwick, R. S., Marty, P., et al. 2001, *A&A*, 369, 1078
 Borkowski, K. J., Reynolds, S. P., Williams, B. J., & Petre, R. 2018, *ApJ*, 868, L21
 Cassam-Chenaï, G., Decourchelle, A., Ballet, J., et al. 2004, *A&A*, 427, 199
 Cunha, K., Hubeny, I., & Lanz, T. 2006, *ApJ*, 647, L143
 Dobashi, K., Uehara, H., Kandori, R., et al. 2005, *PASJ*, 57, S1
 Gotthelf, E. V., Helfand, D. J., & Newburgh, L. 2007, *ApJ*, 654, 267
 Güver, T., & Özel, F. 2009, *MNRAS*, 400, 2050
 Hitomi Collaboration (Aharonian, F., et al.) 2018, *PASJ*, 70, 14
 Katsuda, S., Acero, F., Tominaga, N., et al. 2015, *ApJ*, 814, 29
 Kothes, R. 2013, *A&A*, 560, A18
 Koyama, K., Petre, R., Gotthelf, E. V., et al. 1995, *Nature*, 378, 255
 Koyama, K., Kinugasa, K., Matsuzaki, K., et al. 1997, *PASJ*, 49, L7
 Pannuti, T. G., Allen, G. E., Houck, J. C., & Sturmer, S. J. 2003, *ApJ*, 593, 377
 Park, S., Mori, K., Kargaltsev, O., et al. 2006, *ApJ*, 653, L37
 Park, S., Kargaltsev, O., Pavlov, G. G., et al. 2009, *ApJ*, 695, 431
 Picquenot, A., Acero, F., Bobin, J., et al. 2019, *A&A*, 627, A139
 Picquenot, A., Acero, F., Holland-Ashford, T., Lopez, L. A., & Bobin, J. 2021, *A&A*, 646, A82
 Picquenot, A., Williams, B. J., Acero, F., & Guest, B. T. 2023, *A&A*, 672, A57
 Roberts, D. A., Goss, W. M., Kalberla, P. M. W., Herbstmeier, U., & Schwarz, U. J. 1993, *A&A*, 274, 427
 Sano, H., Fukuda, T., Yoshiike, S., et al. 2015, *ApJ*, 799, 175
 Seward, F. D., Gorenstein, P., & Smith, R. K. 2006, *ApJ*, 636, 873
 Slane, P., Gaensler, B. M., Dame, T. M., et al. 1999, *ApJ*, 525, 357
 Slane, P., Helfand, D. J., van der Swaluw, E., & Murray, S. S. 2004, *ApJ*, 616, 403
 Stephenson, F. R. 1971, *QJRAS*, 12, 10
 Wang, Z. R., Qu, Q. Y., & Chen, Y. 1997, *A&A*, 318, L59
 Williams, B. J., Hewitt, J. W., Petre, R., & Temim, T. 2018, *ApJ*, 855, 118